Available online at www.sciencedirect.com
ScienceDirect
Nuclear Physics B (Proc. Suppl.) 166 (2007) 184–202
NUCLEAR PHYSICS B PROCEEDINGS SUPPLEMENTS
www.elsevierphysics.com

Modeling of the Martian Environment for Radiation Analysis

G. De Angelis[a], F.F. Badavi[b], S.R. Blattnig[c], M.S. Clowdsley[c], J.E. Nealy[d], G.D. Qualls[c], R.C. Singleterry[c], R.K. Tripathi[c], and J.W. Wilson[c]

[a]Istituto Superiore di Sanit, Rome, I-00161, Italy

[b]Christopher Newport University, Newport News, VA 23606, USA

[c]NASA Langley Research Center, Hampton, VA 23681, USA

[d]Old Dominion University, Norfolk, VA 23508, USA

Results for the radiation environment to be found on the planet Mars due to Galactic Cosmic Rays (GCR) and Solar Particle Events (SPE) has been obtained. Primary particle environments computed for Martian conditions are transported within the Mars atmosphere, modeled in a time-dependent way in terms of density, pressure, and temperature vs. altitude, down to the surface, with topography and backscattering patterns taken into account. The atmospheric chemical and isotopic composition has been modeled over results from the in-situ Viking Lander measurements for both major and minor components. The surface topography has been determined by using a model based on the data provided by the Mars Orbiter Laser Altimeter (MOLA) instrument on board the Mars Global Surveyor (MGS) spacecraft. The surface itself has been modeled in both the dry ('regolith') and volatile components. Mars regolith composition has been modeled based on the measurements obtained with orbiter and lander spacecraft from which an average composition has been derived. The volatile inventory properties, both in the regolith and in the seasonal and perennial polar caps, has been taken into account by modeling the deposition of volatiles and its variations with geography and time all throughout the Martian year, from results from imaging data of orbiter spacecraft. Results are given in terms of fluxes, doses and LET, for most kinds of particles, namely protons, neutrons, alpha particles, heavy ions, pions, and muons for various soil compositions.

1. Introduction

Manned space activities have been until present time limited to the near-Earth environment, most of them to low Earth orbit (LEO) scenarios, with only some of the Apollo missions targeted to the Moon. In current times most human exploration and development of space (HEDS) activities are related to the development of the International Space Station (ISS), and therefore take place in the LEO environment. A natural extension of HEDS activities will be going beyond LEO, and reach asteroids, Mars, Jupiter, Saturn, the Kuiper belt and the outskirts of the Solar System [1]. Deep space human exploration activities have been recently boosted in the new US vision for space exploration in the 21st Century, a broad range of human and robotic missions to the Moon, Mars and beyond [2]. The return to the Moon, seen as an outpost, will be only the first step on the way to Mars. Journeys to Mars, as any other space journey outside the protective umbrella of the geomagnetic field, will require higher levels of protection from the radiation environment found in the deep space [3]. The radiation protection is now one of the two NASA highest concerns and priorities [4]. Tools integrating different radiation environments with shielding computation techniques especially tailored for deep space mission scenarios are instrumental in view of this exigency [5].

In view of manned missions targeted to Mars (for a review see e.g. [1]), for which radiation exposure is one of the greatest problems and challenges to be tackled [3,6], it is of fundamental importance to have available a tool which allows to know which are the particle flux and spectra at any time at any point of the Martian surface.

0920-5632/$ – see front matter
doi:10.1016/j.nuclphysbps.2006.12.035

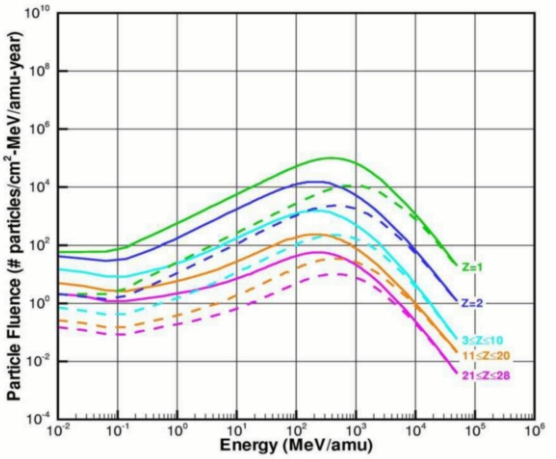

Figure 1. GCR particle environment during the 1977 solar minimum (full lines) and the 1990 solar maximum (dashed lines) in free space at 1 AU distance from the Sun [3].

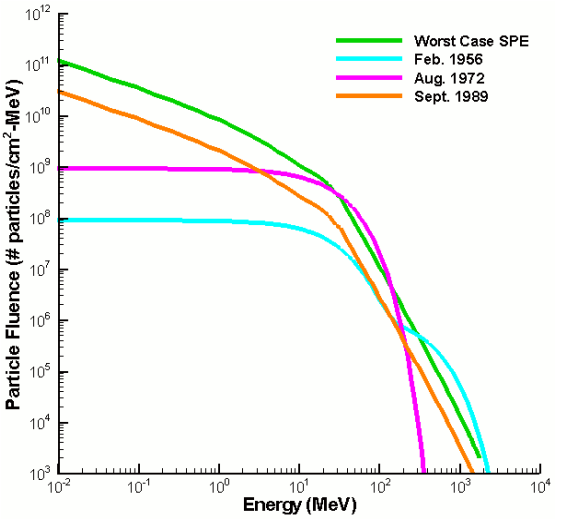

Figure 2. Proton environment for various SPE events in free space at 1 AU distance from the Sun.

With this goal in mind, a new model for the radiation environment due to Galactic Cosmic Rays (GCR) and Solar Particle Events (SPE) to be found on the planet Mars has been developed. Galactic and solar primary particles rescaled for Mars conditions are transported within the Martian atmosphere, with temporal properties modeled with variable timescales, down to the surface, with altitude and backscattering patterns taken into account. The tool allows analysis for manned Mars landing missions (e.g. [1]), as well as planetary science studies, e.g. subsurface water and volatile inventory studies (e.g. [7]). This radiation environment is based on the Mars model by De Angelis et al. ([6,8]), with a detailed description of the Martian surface with different soil compositions including ices and volatiles. Radiation analysis work was performed with this environmental model ([6],[8-11]). In this work the model from De Angelis et al. [6,8] is extended: the older model allow computing a radiation environment only on the planet surface, whereas this model allow computing at any location within the atmosphere: backscattered particles are transported from the surface through the atmosphere. The particle data and the techniques used to model the Mars environment have been presented in [9,11], and will be only briefly addressed in this paper. The emphasis of this paper is on results, in terms of fluxes, doses and LET for most kinds of particles, namely protons, neutrons, alpha particles, heavy ions, pions, and muons for various soil compositions. The analysis for the pions and muons component is more extensively described in the companion paper [10]. These models have been, are and will be used as a planning tool for most ongoing and future Mars-targeted missions (e.g. MSL, PHOBOS-GRUNT, NASA manned vehicles, etc.), as well as for the design and development of spacecraft payload instrumentation (e.g. instruments for MSL, LIULIN-F for PHOBOS-GRUNT, etc.).

2. Particle environmental Models

2.1. Galactic Cosmic Rays (GCR)

Galactic Cosmic Rays (GCR) originate outside our Solar System in ways not totally clear yet [12,13]. They are composed of highly energetic, fully ionized nuclei of all charges from hydrogen to uranium, with a large decrease in the intensity of particles with charge higher than 28 [14].

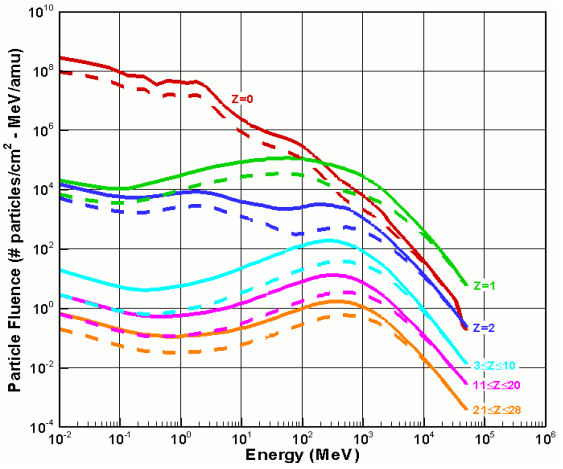

Figure 3. GCR particle environment during the 1977 solar minimum (full lines) and the 1990 solar maximum (dashed lines) on the Martian surface with regolithic soil.

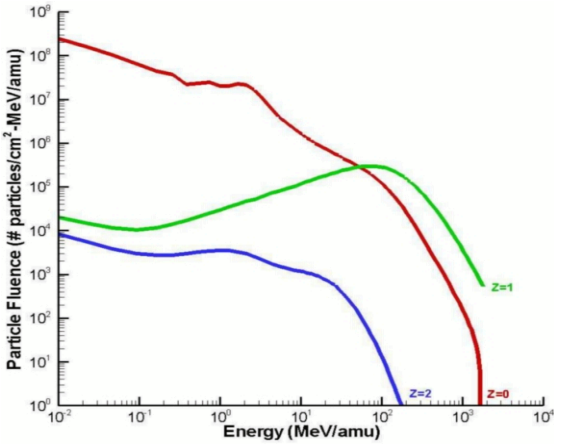

Figure 4. The Martian surface radiation environment during the September 1989 SPE (regolithic soil).

From interstellar space the GCR enter the Solar System, where they come into contact with the particles of the solar wind, which transports the solar magnetic field away from the Sun [15]. The distribution of cosmic rays in the heliosphere depends on time, position and particle magnetic rigidity, and complies with the transport equation by Parker [16], a solution of the Fokker-Planck equation in which the inward diffusion of galactic cosmic rays is balanced by the solar wind outward convection, assuming a spherically symmetric heliosphere and an isotropic cosmic ray particles flux. Processes included in the equation are the GCR convection by the solar wind, their drift in the inhomogeneous heliospheric field, the anisotropic diffusion in the interplanetary magnetic field irregularities, and the adiabatic energy losses caused by the divergence of these irregularities [17]. At a time the cosmic ions density within the solar system is related to the GCR density outside the Solar System as:

$$\mu(r,R) = \mu_0(R)\ exp\left[-\int_r V(r')dr'/D(r',R)\right] \quad (1)$$

where $D(r,R)$ is the diffusion coefficient, $\mu(r,R)$ is the ion density at radial distance r and magnetic rigidity R (particle momentum per unit charge and determines the trajectory radius of curvature in a magnetic field), $\mu_0(R)$ is the density in interstellar space, and $V(r)$ is the solar wind speed [18]. The time dependence due to solar activity of the variations of the solar wind velocity and diffusion coefficient is taken into account with the statistical model developed by Wilson et al. [19,20] relating the sunspot number to the cosmic ray induced neutron monitor count rate measured at the Deep River location, Ontario, Canada. The GCR cosmic ray density rescaling for distance is performed in this work, as in previous work [20,21], with the simplified model by Badhwar et al. [22], in which the solar wind velocity is kept constant at 400 km/s and the diffusion coefficient only is taken as a function of time and correlated with the Mt. Washington neutron monitor count rate, with the diffusion patterns only dependent on the orientation of the solar magnetic dipole. Assuming an isotropic diffusion coefficient increasing with radial distance as $D(r,R) = D0(R)rs$ where s is on the order of 0 to 2, all these assumptions lead to:

$$\mu(r,R) = \mu_0(R)exp\left[-V_0\frac{r_0^{1-s} - r^{1-s}}{(1-s)D_0(R)}\right] \quad (2)$$

where V_0 ,r_0, and $D_0(R)$ are the wind speed, size of the modulation cavity (50 to 100 AU), and diffusion coefficient at 1 AU respectively. Studies of the solar modulation patterns performed by using data from Pioneer, Voyager, and IMP spacecraft show variability of s with solar cycle for some restricted energy ranges, but a value for the s coefficient of s = 0.5 gives a good representation of the gross GCR behavior for all energies above 70 MeV [23]. The spectra for GCR at 1 AU from the Sun for solar maximum and minimum is shown in Fig.1. The flux difference between 1 AU and the distance of Mars is at most a few percent [6,24].

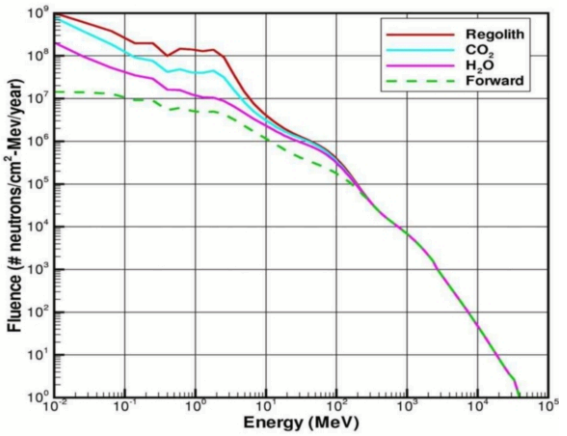

Figure 5. Neutron fluence during the 1977 solar minimum at the Martian surface with various soil compositions (the "forward" component is for regolithic composition).

2.2. Solar Particle Events (SPE)

The Sun has been known for long time as a prolific source of energetic particles, with the first detection of solar particles by Forbush [25] as early as in 1946 leading to the name 'solar cosmic rays'. Various short-term cosmic ray flux increases have been observed shortly afterwards at the ground level in direct association with solar flares [26-28], mostly as ground level ionization rate increases, and the largest event, that of 23 February 1956, was analyzed in detail through neutron monitor data [29,30]. The analysis of the particle flux of the 23 February 1956 solar particle event showed that only the solar magnetic field was capable of accelerating protons in the amounts and to the energies detected in the event [31]. This conclusion is still valid today whether or not the particles are produced within solar flares or within coronal mass ejections, forming a bow shock transition region which the most recent opinions consider the most likely place where particle acceleration occurs, with the energy in both cases from the same magnetic field [32-34].

In order to take into account solar particle events in space mission radiation shielding analysis, three main issues are to be considered, namely fluence, frequency distribution, expected flux and energy spectra, and the largest likely event to be encountered during the mission [35]. The greatest concern given by Solar Particle Events is due to our inability to predict their occurrence [36]. Only few events of very large size can give appreciable consequences for deep space radiation shielding analysis [35], namely events with fluence of protons with energy $E > 10MeV$ larger than 3 x $107/cm^2$. The rate of occurrence of such events is discussed in [37]. An average event could provide a neutron monitor count rate increase lower than a factor 1.5, whereas in the event of 23 February 1956, the largest yet observed, the neutron monitor count rates increased of 36 times above the background level. The second largest event ever observed was that of 29 September 1989, with a measured neutron monitor count rate 370 percent over background [38]. No other events of such magnitude have ever been observed, apart from the 12 November 1960 and the August 1972 events [39], indeed having narrower energy spectra compared with the 1989 event, especially with respect to higher energies, the most relevant in this respect [40]. From a model by Nymmik [41] it comes out that the event of 29 September 1989 just for protons with energy $E > 30$ MeV had a fluence of 1.4 x $109/cm^2$ protons, so about 50 times larger than the threshold mentioned above. Due to the exceptionality of the 1956 event, and the comparability of other large events, and the more extended spectrum, compared to the other events, a worst-case strat-

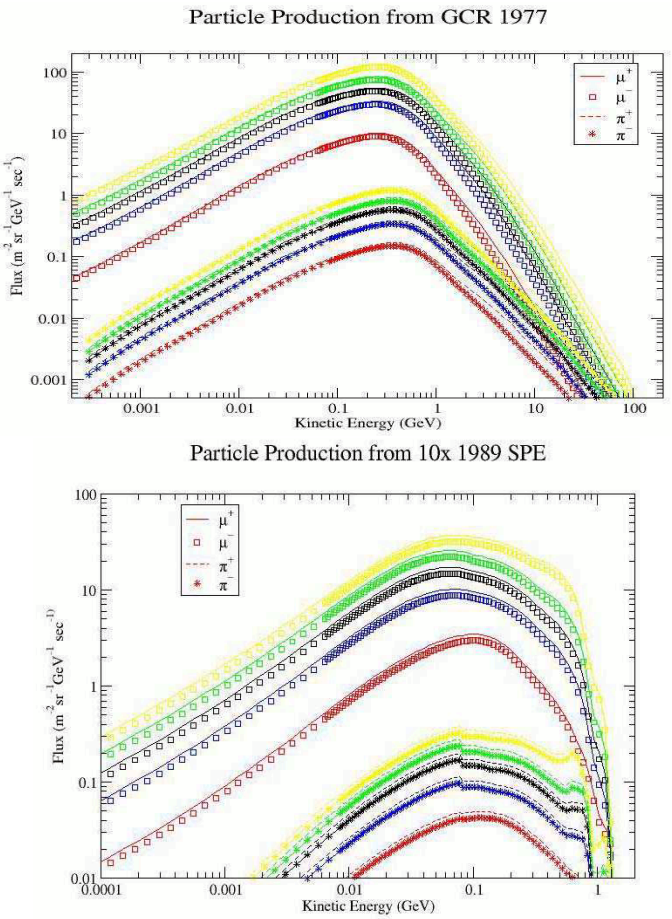

Figure 6. Pions and muons due to GCR in 1977 solar minimum and due to 10*1989 SPE on the Martian surface with regolithic soil (from Ref. [10]).

egy based on a multiple of the 29 September 1989 event seems to be quite suitable to the needs of radiation analysis [42].

The radial dependence of the particle flux of SPE is very poorly known, and seems to depend on the characteristics of the interplanetary magnetic field through which these particles go [35], with events generated by the shock regions of a CME may decrease little between 1 AU to Mars orbit or even further, whereas the Gauss law seems appropriate at large distances from the sun [24]. The SPE particles are generally controlled all throughout the solar system by the flux tubes of the solar wind Archimedes spiral [35], so for a well field line connected event the particle flux radial dependence [35] should be as steep as $r = -3.3$. For the needs of a radiation shielding analysis, an event four times larger than the 29 September 1989 event [42] which is likely to be exceeded only 1 percent of the time [43] is used, with a simple inverse r (i.e. r = -1) dependence for every spacecraft distance from the sun, to obtain an upper limit for the dose given by the event occurrence. The proton SPE spectrum is shown in Fig. 2 for various solar events.

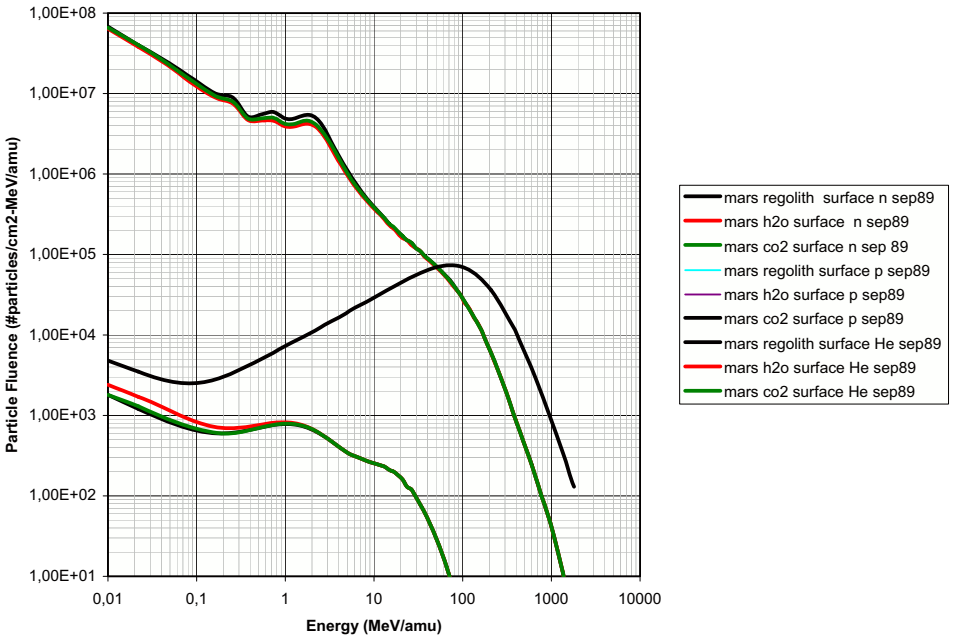

Figure 7. Particle fluence from 1989 SPE at the Martian surface with various soil composition

3. Planetary Environmental Models

3.1. Planetary Surface and Subsurface Environments

A planetary target body, i.e. a planet or one of its satellites, needs to be modeled to assess the radiation dose a crew will intake during the surface activities. If the body is atmosphereless, it has to be modeled in position (astrometry), size, topography, and surface chemical composition, to get the atomic surface composition needed for transport computation, to evaluate the backscattering radiation component, especially neutrons. If the target body has an atmosphere, a profile of the atmosphere in terms of density, temperature and composition vs. altitude (and time) should be provided, to compute how the primary particle fluxes are modified by the interaction with the atmosphere. The knowledge of the target body topography is particularly important in the case an atmosphere is present, to properly evaluate the thickness down to which the effects of the atmosphere have to be taken into account. In the Solar System bodies (see, e.g. [44]) two kinds of surface composition are prevalent, namely a silicatic rocky composition on the bodies of the Inner Solar System (i.e. Mercury, Venus, the Earth, the Moon, Mars and its satellites, asteroids), and a mostly icy (water ice, methane ice, ammonia ice) composition of the solid bodies of the Outer Solar System (satellites of Jupiter, Saturn, Uranus, Neptune, Pluto with his moon Charon, comets, the Kuiper Belt and all Trans-Neptunian objects). The giant planets of the Outer Solar System have a gaseous composition all along their body (Jupiter, Saturn, Uranus, Neptune), and seem not to have any solid surface [45] on which any surface activity looks to be practicable. Interesting phenomena take place on the surface of bodies with locally mixed rock/ice composition, like in planets with seasonal or perennial volatile-generated polar caps, like e.g. the carbon dioxide ice and water ice caps on Mars [6], as well as at any interface, like atmosphere-surface, space-surface, surface-subsurface, regolith-bedrock, etc. [46].

Neutron backscattering from silicatic surface is important particularly at the lower energies [47],

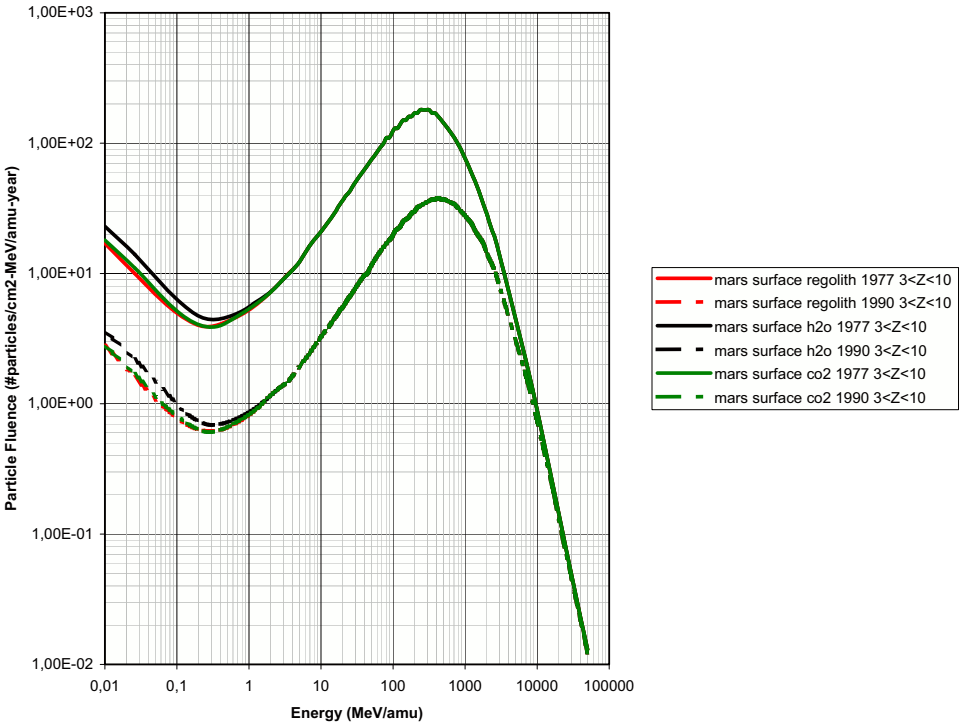

Figure 8. GCR environment, for ions with $3 < Z < 10$, during the 1977 solar minimum (full lines) and the 1990 solar maximum (dashed lines) on the Martian surface with various soil compositions.

whereas the interaction with ices produces far less neutrons [24]. In free space, the particle environment is the same as shown above. At the surface, the particle environment undergoes two main modifications with respect to that found in free space: the primary particles are limited to come only from above the surface, so the solid angle of acceptance of primary particles is limited to 2 , and it is not the full 4 solid angle like in the free space case. In some cases, due to local topography features like valleys or craters, the solid angle might be even smaller than 2 [48]. Moreover, the backscattering component, mostly neutrons, created by the interaction between the incoming particles and the nuclei composing the surface, is to be added to the particle flux at the surface.

For atmosphereless bodies this component is about 1% of the dose given by GCR alone [21], with little dependence on the composition of the surface materials. For target bodies with an atmosphere, a profile of the atmosphere in terms of density, temperature and composition vs. altitude (and time) should be provided, to compute how the primary particle fluxes are modified by atmospheric interactions. At the surface the modified particle fields interact with the nuclei composing the surface, whose physical conditions and chemical composition should be known with depth in order to evaluate the backscattered radiation.

3.2. The Mars Physico-Chemical Model

This Martian physico-chemical environmental model has been developed in successive phases ([6],[8-11]). Mars is a planet with an atmosphere, so the modeling of the Martian radiation environment has to deal with both atmospheric and surface properties.

The Martian atmosphere has been modeled by using the Mars Global Reference Atmospheric Model - version 2001 ('Mars-GRAM 2001', [49]),

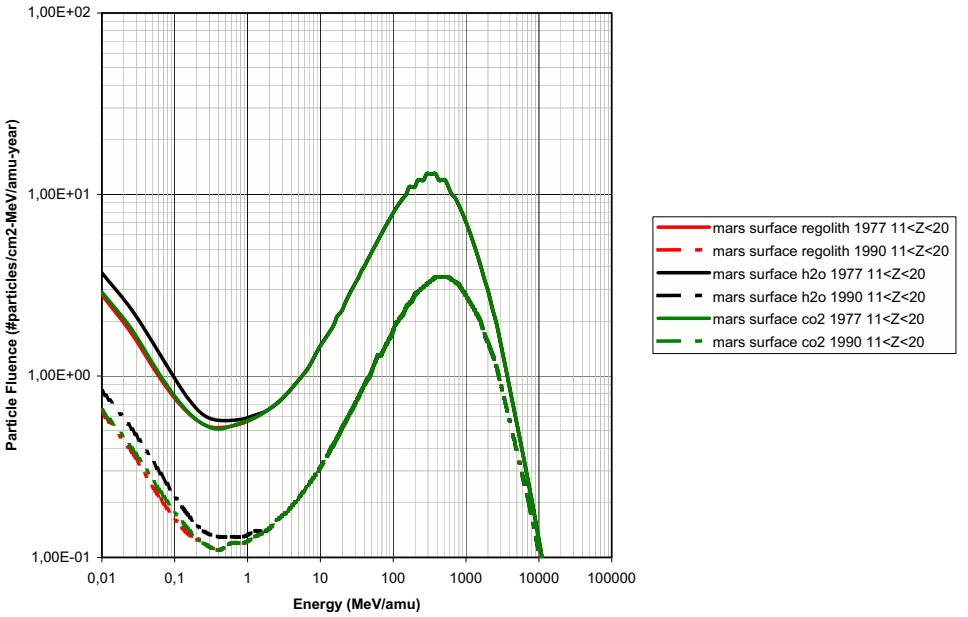

Figure 9. GCR environment, for ions with $11 < Z < 20$, during the 1977 solar minimum (full lines) and the 1990 solar maximum (dashed lines) on the Martian surface with various soil compositions.

based on input data generated as output of the NASA Ames Mars General Circulation Model (MGCM) for the lower atmosphere, from the surface to 80 km altitude [50,51], the University of Arizona Mars Thermosphere General Circulation Model (MTGCM) for the higher atmosphere, from 80 km to 170 km altitude [52,53], and a modified Stewart-type thermospheric model, i.e. a latitude-longitude dependent parametric model also depending on solar activity [54], above 170 km altitude. This model can provide at any time a profile of the Martian atmosphere in terms of density, pressure, and temperature vs. altitude, needed to compute the atmosphere thickness for the incoming particle flux. The atmospheric chemical and isotopic composition has been modeled over results from the in-situ Viking Lander measurements for both major [55]and minor [56] components (see Table 1). The surface altitude, or better the atmospheric depth for incoming particles, to compute the atmospheric thickness profile has been determined by using a model for the Martian topography based on the data provided by the Mars Orbiter Laser Altimeter (MOLA) instrument on board the Mars Global Surveyor (MGS) spacecraft [57].

CO_2	95.32 %
N_2	02.70 %
Ar	01.60 %
O_2	00.13 %
CO	00.08 %

Table 1
Adopted chemical composition for the Martian atmosphere

The MOLA topography is measured with respect to a zero elevation surface level known as the MOLA aeroid [58], which is defined as the gravitational equipotential surface whose average value at the equator is equal to the mean planetary radius determined by MOLA data. Among the various data resolution available [59], in this work half-degree latitude-longitude resolution data for both MOLA aeroid surface and topography have been used (i.e. 30 km spatial resolution at the equator), but this value can be tuned in case of different user needs. The Mars regolith composition has been modeled based on av-

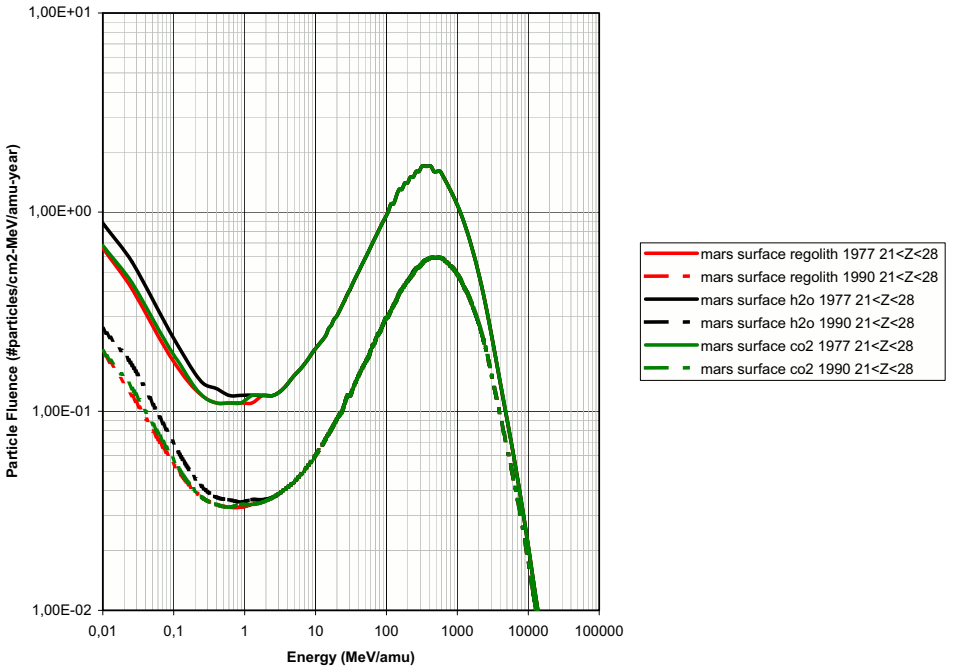

Figure 10. GCR environment, for ions with $21 < Z < 28$, during the 1977 solar minimum (full lines) and the 1990 solar maximum (dashed lines) on the Martian surface with various soil compositions.

erages over the measurements obtained for Mars 5 [60] and Phobos 2 [61,62] with gamma-ray spectroscopy, and at the various landing sites Viking Landers 1 and 2 [63,64] and Mars Pathfinder missions [65,66]. From the averaging process an average composition has been obtained (see Table 2).

SiO_2	44.2 %
FeO	16.8 %
Al_2O_3	8.8 %
CaO	6.6 %
MgO	6.2 %
SO_3	5.5 %
Na_2O	2.5 %
TiO_2	1.0 %

Table 2
Adopted chemical composition for the Martian surface (regolithic soil component)

This surface geochemical model got validated by the Mars Exploration Rovers: the geochemical and mineralogical data from Spirit and Opportunity [67-71] show a stunning similarity with the data from this model, with soil compositional differences at most of a few percent, even 1% in some cases. In this first project a value of 1.6 g/cm^3 [72] for the Mars soil density has been adopted. The composition, different with respect to the regolith (e.g. CO_2 ice, H_2O ice), of seasonal and perennial polar caps [73] has been taken into account by modeling the deposition of the possible volatile inventory over the residual caps, along with its geographical variations all throughout the Martian year, for both the Mars North [74,75] and South Pole [76,77], from results from imaging data of orbiter spacecraft. No such 3D Mars time dependent polar caps modeling was previously available for radiation analysis purposes. The importance of having a time-dependent soil composition model is below.

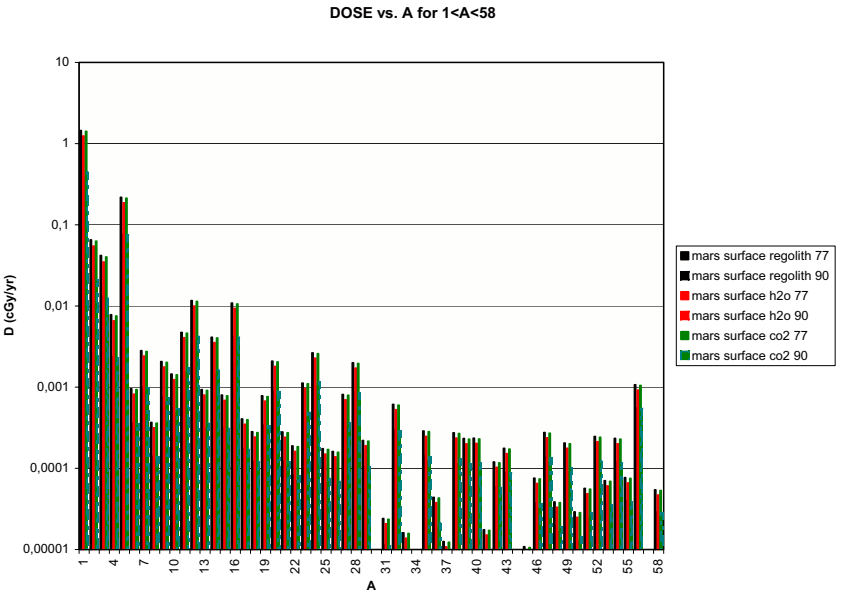

Figure 11. Dose for each ion with $1 < A < 58$ during the 1977 solar minimum and the 1990 solar maximum on the Martian surface with various soil compositions.

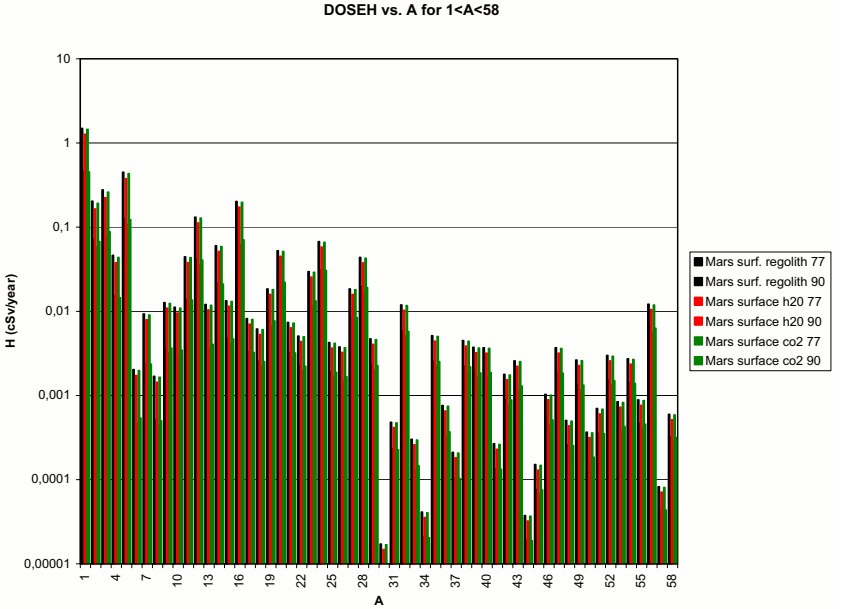

Figure 12. Dose equivalent for each ion with $1 < A < 58$ during the 1977 solar minimum and the 1990 solar maximum on the Martian surface with various soil compositions.

Regolith				Water Ice				Carbon dioxide ice			
D (cGy/yr)		H (cSv/yr)		D (cGy/yr)		H (cSv/yr)		D (cGy/yr)		H (cSv/yr)	
1977	1990	1977	1990	1977	1990	1977	1990	1977	1990	1977	1990
6.90	2.80	29.30	11.86	3.40	1.40	12.04	4.78	4.40	1.70	16.50	6.42

Table 3
Induced Dose (D) and Dose Equivalent (H) at Martian surface for different soil compositions.

Atmosphere (h=7 km)				Surface (regolith)			
D (cGy/yr)		H (cSv/yr)		D (cGy/yr)		H (cSv/yr)	
1977	1990	1977	1990	1977	1990	1977	1990
5.80	2.00	6.40	2.19	6.90	2.80	29.30	11.86

Table 4
Induced Dose (D) and Dose Equivalent (H) at-7km-altitude vs. at-Martian-surface for regolithic soil compositions.

Regolith				Water Ice				Carbon dioxide ice			
D (cGy/yr)		H (cSv/yr)		D (cGy/yr)		H (cSv/yr)		D (cGy/yr)		H (cSv/yr)	
1977	1990	1977	1990	1977	1990	1977	1990	1977	1990	1977	1990
1.84	0.60	3.30	1.09	1.58	0.50	2.80	0.93	1.80	0.60	3.20	1.06

Table 5
Total Dose (D) and Dose Equivalent(H) at Martian surface from all charged particles with Z=1,28 for different soil compositions.

4. Radiation transport computing tools

The transport of positive charged particles, i.e. protons and heavier ions, have been performed with a current version of the NASA Langley Research Center (LaRC) heavy ion deterministic code HZETRN [78], which provides particle energy spectra at predefined positions in the material layer of interest as well as the pertinent dosimetric quantities, with energy deposition from both primary and secondary particles, including nuclear target fragments, accounted for.

The materials are modeled as a thickness file including distance of each material traversed in the order progressing from the outer boundary inward toward the target point. With the specified environment, i.e. the specified charged particle flux boundary conditions, the transport code is used to generate dose vs. depth functions for each material under consideration over a range of thickness adequate for interpolation for the shielding analysis. Primary particles at planet distances at intermediate time between solar minimum and maximum epochs are obtained as discussed above, through the simplified diffusion model by Badhwar et al. [22], adopting for the coefficient the value of s = 0.5. The diffusion coefficient (x) is then computed as:

$$\alpha(x) = (r_e^{1-s} - r_p^{1-s}) \{ln[h(x, r_e)] - ln[h(x, r_p)]\} \quad (3)$$

where re is the distance between the Earth and the Sun (1 AU), computed from the center of the planet, r_p is the cm2 distance between the Sun and the target planet, r is the shielding thickness for which the dose is computed, and $h(x, r)$ is the dose at thickness x and distance r from the Sun. So to compute the dose at each distance r from the Sun

$$h(x,r) = h(x,r_e) \cdot \cdot exp\left[\alpha(x)(r^{1-s} - r_e^{1-s}\right] \quad (4)$$

The same transport code, HZETRN, is used for transport calculations of positive SPE particles.

5. Results

The radiation environment at a location at the surface of Mars is shown for GCR at solar 1977 solar minimum and 1990 solar maximum in Fig. 3 and regarding SPE in Fig. 4 for the solar particle event of September 29, 1989. Both results are shown for regolithic soil. The particles with 'Z=0' in both figures are the albedo neutrons generated by the interaction of the primary particles with the surface [5], with a much higher energy tail than for atmosphereless bodies [5,79]. The effect of the atmosphere is very evident on the particle transport, with a high energy tail component for neutrons generated by the atmospheric transport [80], tail that is absent in the particle transport on an atmosphereless body [79].

Results have been obtained for various kinds of particles and for different surface compositions: only the latitudes closer to the equator the soil is mostly silicatic regolith, whereas for northern and southern locations a suitable mix of ices of water and carbon dioxide needs to be used [6]. For sake of brevity it is impossible to show all available results for both GCR and SPE environments and different soils. As the most significant examples, fluences for protons, neutrons, heavy ions, pions and muons are shown in Figs. 5-10. The different soil composition explains the much lower neutron production by the water ice than the silicatic regolith. Dose and dose equivalents for different scenarios are shown in Figs. 11-13 and Tables 3-5.

A radiation flux, dose and a dose rate can be computed at any time at any location on the planet. As an example, a Mars high neutron radiation environment map [6], the tail created by atmospheric particle transport [5,79], due to GCR for 1977 Solar Minimum conditions is shown in Fig. 14, with a striking correspondence between neutron flux and Mars topography (shown in Fig.15), putting clearly into evidence the effects of even this so tenuous atmosphere on particle transport. The effects of layer superposition due to seasonal polar caps modifications is evident in Fig. 16, where the neutron fluxes in different Mars regions are variable with the season due to surface composition changes.

These doses are slightly higher (about 20%) than those from [81], obtained with a simplified model of the Martian atmosphere.

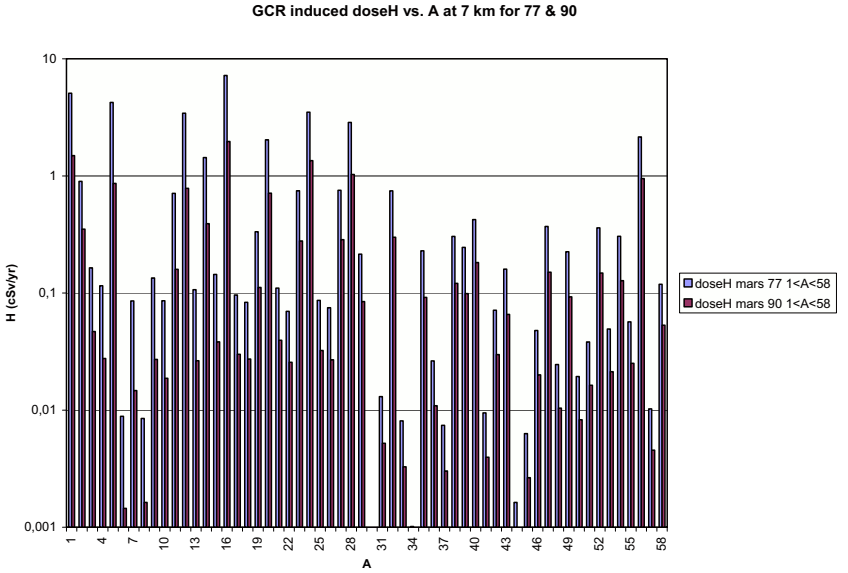

Figure 13. Dose equivalent for each ion with $1 < A < 58$ during the 1977 solar minimum and the 1990 solar maximum at an altitude of 7 km from the Martian surface (downward particles only).

6. Conclusions

An updated and extended new model for the radiation environment to be found on Mars (above and on the surface) due to Galactic Cosmic Rays (GCR), Solar Particle Events (SPE) and backscattering effects has been developed. Results for fluxes, doses and dose equivalents have been given. This Mars Radiation Environment Model will be tested against the data from spacecraft instruments in the near future.

7. Acknowledgments

The authors are indebted with K.Y. Fan, S.H. Husch and W.A. Mickley, for their invaluable help. This work has been performed under the NASA Research Grant NCC-1-404.

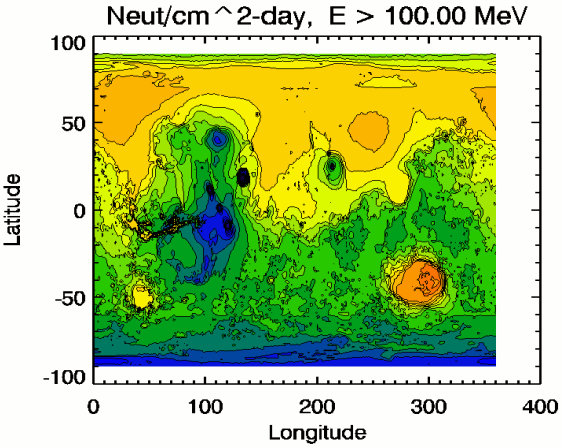

Figure 14. Map of high energy neutron integral flux on the Mars surface for GCR at 1977 Solar Minimum.

REFERENCES

1. Hoffman, S.J., and D.I. Kaplan, Human Exploration of Mars: the Reference Mission of the NASA Mars Exploration Study Team, NASA SP-6107 (1997).
2. Bush, G.W., A Renewed Spirit of Discovery - The President's Vision for U.S. Space Exploration, Washington (2004).
3. Cucinotta, F.A., W. Schimmerling, J.W. Wilson, L.E. Peterson, G.D. Badhwar, P.B. Saganti, and J.F. Dicello, Space radiation cancer risks and uncertainties for Mars mis-

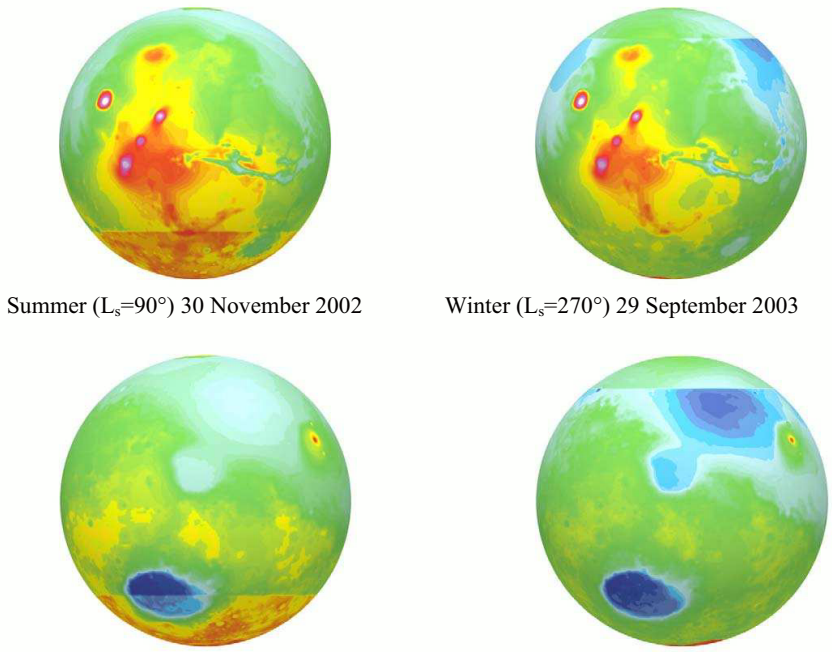

Figure 16. Variability of neutron fluxes in different Mars regions with the season due to surface composition.

sions, Radiat. Res., 156, 682-688 (2001).
4. O'Keefe, S., Administrator O'Keefe Pitches His Vision for NASA, http://www.spaceflightnow.com/news/n0203/27okeefe/ (2002).
5. De Angelis, G., M.S. Clowdsley, J.E. Nealy, R.C. Singleterry, R.K. Tripathi, and J.W. Wilson, Radiation Shielding Analysis for Deep Space Missions, in Proceedings of the Space Technology and Application International Forum (STAIF-2003) 'Expanding the Frontiers of Science', edited by M. El-Genk, AIP Conference Proceedings, New York, pp. 972-983 (2003).
6. De Angelis, G., M.S. Clowdsley, R.C. Singleterry, and J.W. Wilson, A new Mars radiation environmental model with visualization, Adv. Space. Res., 34, 1328-1332 (2004).
7. Carr, M.H., Water on Mars, Oxford University Press, New York, 1996.
8. De Angelis, G., M.S. Clowdsley, R.C. Singleterry, and J.W. Wilson, A new time-dependent model for the Martian radiation environment, Sixth International Conference on Mars, July 20-25 2003, Pasadena CA, Abstract no. 3249 (2003).
9. De Angelis, G., J.W. Wilson, M.S. Clowdsley, G.D. Qualls, and R.C. Singleterry, Modeling of the Martian environment for radiation analysis, Adv. Space. Res., submitted.
10. Blattnig, S.R., G. De Angelis, R.B. Norman, J.W. Norbury, and F.F. Badavi, Preliminary analysis of pion and muon radiation on Mars, Adv. Space. Res., submitted.
11. De Angelis, G., F.F. Badavi, S.R. Blattnig, M.S. Clowdsley, G.D. Qualls, R.C. Singleterry, and J.W. Wilson, Radiation environment modeling for the planet Mars, Paper SAE-2005-01-2832, pp. 1-15, Society for Automotive Engineering (SAE) (2005).
12. Hall, D. L., M.L. Duldig, and J.E. Humble, Analysis of sidereal and solar anisotropies in cosmic Rays, Space Sci. Rev., 17, 401-442 (1996).
13. Droege, W., Particle Scattering by Magnetic Fields, in Cosmic Rays and Earth, edited by

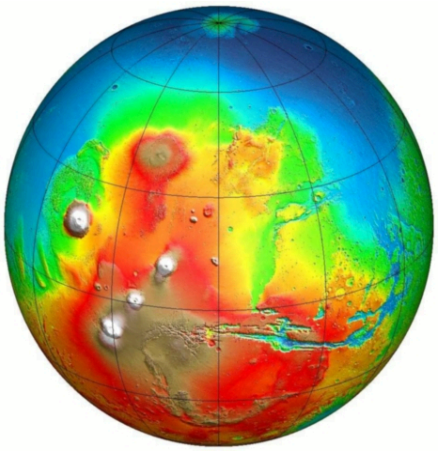

Figure 15. Mars topographic map from MOLA data [57].

J.W. Bieber, E. Eroshenko, P. Evenson, E.O. Flueckiger, and R. Kallenbach, pp. 121-152, Kluwer Academic Publisher, Dordrecht, The Netherlands (2000).
14. Badhwar, G.D., Free Space Radiation Environment, in Risk Evaluation of Cosmic-Ray Exposure in Long-Term Manned Space Mission, edited by K. Fujitaka, H. Majima, K. Ando, H. Yasuda, and M. Suzuki, pp. 17-32, Kodansha Scientific Ltd., Tokyo, Japan (1999).
15. Badhwar, G.D., and P.M. O'Neill, Galactic cosmic radiation model and its applications, Adv. Space Res., 17, 7-17 (1996).
16. Parker, E. N., The passage of energetic charged particles through interplanetary space, Planet. Space Sci., 13, 9-49 (1965).
17. Belov, A., Large Scale Modulation: View from the Earth, in Cosmic Rays and Earth, edited by J.W. Bieber, E. Eroshenko, P. Evenson, E.O. Flueckiger, and R. Kallenbach, pp. 79-106, Kluwer Academic Publisher, Dordrecht, The Netherlands (2000).
18. Balasubrahmanyan, V.K., E. Boldt, and R. Palmeira, Solar modulation of galactic cosmic rays, J. Geophys. Res., 72, 27-36 (1967).
19. Wilson, J.W., M.H.Y. Kim, F.A. Cucinotta, F.F. Badavi, J.L. Shinn, H. Tai, G.D. Badhwar, and W. Atwell, Solar Cycle Variations and Application to the Space Radiation Environment, NASA TP-209369 (1999).
20. Wilson, J.W., F.F. Badavi, M.H.Y. Kim, M.S. Clowdsley, J.H. Heinbockel, F.A. Cucinotta,, G.D. Badhwar, W. Atwell, and S.L. Huston, Natural and Induced Environment in Low Earth Orbit, NASA/TM-2002-211668 (2002).
21. Wilson, J.W., J.L. Shinn, R.K. Tripathi, R.C. Singleterry, M.S. Clowdsley, S.A. Thibeault, F.M. Cheatwood, W. Schimmerling, F.A. Cucinotta, G.D. Badhwar, A.K. Norr, M.H.Y. Kim, F.F. Badavi, J.H. Heinbockel, J. Miller, C. Zeitlin, and L. Heilbronn, Issues in deep space radiation protection, Acta Astronautica, 49, 289-312 (2001).
22. Badhwar, G. D., F.A. Cucinotta, and P.M. O'Neill, An analysis of interplanetary space radiation exposure for various solar cycles, Radiat. Res., 138, 201-208 (1994).
23. Fuji, Z., and F.B. McDonald, Radial intensity gradients of galactic cosmic rays (1972-1995) in the Heliosphere, J. Geophys. Res., 102, 24201-24208 (1997).
24. Wilson, J.W., J.E. Nealy, G. De Angelis, M.S. Clowdsley, and F.F. Badavi, Deep Space Environment and Shielding, in Proceedings of the Space Technology and Application International Forum (STAIF-2003) 'Expanding the Frontiers of Science', edited by M. El-Genk, AIP Conference Proceedings, New York, pp. 993-1009 (2003).
25. Forbush, S.E., Three unusual cosmic-ray increases possibly due to charged particles from the Sun, Phys. Rev., 70, 771-772 (1946).
26. Eliot, H., Progress in Cosmic Ray Physics, North Holland Publishing Company, Amsterdam, The Netherlands (1952).
27. Firor, J., Cosmic radiation intensity - time variations and their origin. IV. Increases associated with solar flares, Phys. Rev., 94, 1017-1028 (1954).
28. Singer, S.F., Progress in Cosmic Ray Physics, North Holland Publishing Company, Amsterdam, The Netherlands, (1958).
29. Meyer, P., E.N. Parker, and J.A. Simpson, Solar cosmic rays of February 1956 and their propagation through interplanetary space,

Phys. Rev., 104, 768-781 (1956).
30. Lst, R., and J.A. Simpson, Initial stages in the propagation of cosmic rays Produced by solar flares, Phys. Rev., 108, 1563-1576 (1957).
31. Parker, E.N., Acceleration of cosmic rays in the solar flares, Phys. Rev., 107, 830-836 (1957).
32. Litvinenko, Y.E., and B.V. Somov, Relativistic acceleration of protons in reconnecting current sheets of solar flares, Solar Phys.,158, 317-330 (1995).
33. Reames, D.V., Particle acceleration at the Sun and in the heliosphere, Space Sci. Rev., 90, 417-491 (1999).
34. Ryan, J.M., J.A. Lockwood, and H. Debrunner, Solar Energetic Particles, in Cosmic Rays and Earth, edited by J.W. Bieber, E. Eroshenko, P. Evenson, E.O. Flueckiger, and R. Kallenbach, Kluwer Academic Publisher, Dordrecht, The Netherlands, pp. 35-53 (2000).
35. Badhwar, G. D., Deep Space Radiation Sources, Models, and Environmental Uncertainties, in Shielding Strategies for Human Space Exploration, edited by J.W. Wilson, J. Miller, A. Konradi, and F.A. Cucinotta, pp. 17-28, NASA CP-3360 (1997).
36. Shea, M.A., and D.F. Smart, Cosmic Ray Implications for Human Health, in Cosmic Rays and Earth, edited by J.W. Bieber, E. Eroshenko, P. Evenson, E.O. Flueckiger, and R. Kallenbach, Kluwer Academic Publisher, Dordrecht, The Netherlands, pp. 187-205 (2000).
37. Shea, M.A., and D.F. Smart, History of Energetic Solar Protons for the Past Three Solar Cycles Including Cycle 22 Update, in Biological Effects and Physics of Solar and Galactic Cosmic Radiation, edited by C. E. Swenberg, G. Horneck, and G. Stassinopoulos, Plenum Press, New York, pp. 37-71 (1993).
38. Lovell, J.L., M.L. Duldig, and J.E. Humble, An extended analysis of the September 1989 cosmic ray ground level enhancement, J. Geophys. Res., 103, 23733-23742 (1998).
39. Shea, M.A., and D.F. Smart, Fifty Years of Cosmic Radiation Data, in Cosmic Rays and Earth, edited by J.W. Bieber, E. Eroshenko, P. Evenson, E.O. Flueckiger, and R. Kallenbach, Kluwer Academic Publisher, Dordrecht, The Netherlands, pp. 229-262 (2000).
40. Nymmik, R.A., Behavioral Features of Energy Spectra of Particles Fluences and Peak Fluxes in Solar Cosmic Rays, in Proceedings of 24th International Cosmic Ray Conference (Rome, Italy), edited by N. Iucci and E. Lamanna, Nuovo Cimento, Rome, Italy, pp. 65-68 (1995).
41. Nymmik, R.A., Models describing solar cosmic ray events, Radiat. Meas., 26, 417-420 (1997).
42. Tripathi, R.K., J.W. Wilson, F.A. Cucinotta, J.E. Nealy, M.S. Clowdsley, and M.H.Y. Kim, Deep Space Mission Shielding Optimization, SAE 2001-01-2326 (2001).
43. Xapsos, M. A., J.L. Barth, E.G. Stassinopoulos, E.A. Burke, and G.B. Gee, Space Environment Effects: Model for Emission of Solar Protons (ESP) - Cumulative and Worst-Case Event Fluences, NASA/TP-1999-209763 (1999).
44. Safronov, V.S., Cosmochemistry of the Moon and Planets, Nauka Publishers, Moscow, USSR (1975). (In Russian)
45. Lewis, J.S., Physics and Chemistry of the Solar System, Academic Press, San Diego CA (1997).
46. De Angelis, G., J.E. Nealy, M.S. Clowdsley, R.K.Tripathi, and J.W. Wilson, Radiation analysis for manned missions to the Jupiter system, Adv. Space. Res., 34, 1395-1403 (2004).
47. Wilson, J.W., M.H.Y. Kim, M.S. Clowdsley, J.H. Heinbockel, R.K. Tripathi, R.C. Singleterry, J.L. Shinn, and R. Suggs, Mars Surface Ionizing Radiation Environment: Need For Validation, paper presented at the Workshop on 'Mars 2001: Integrated Science in Preparation for Sample Return and Human Exploration', Lunar and Planetary Institute, LPI Contribution No. 991, Houston, TX, October, 2-4 (1999).
48. Simonsen, L.C., J.E. Nealy, L.W. Townsend, and J.W. Wilson, Radiation Exposure for Manned Mars Surface Missions, NASA TP-

2979 (1990).
49. Justus, C.G., and D.L. Johnson, Mars Global Reference Atmospheric Model 2001 Version (Mars-GRAM 2001), NASA TM-2001-210961 (2001).
50. Haberle, R.M., J.B. Pollack, J.R. Barnes, R.W. Zurek, C.B. Leovy, J.R. Murphy, H. Lee, and J. Schaeffer, Mars atmospheric dynamics as simulated by the NASA Ames General Circulation Model. I - The zonal-mean circulation, J. Geophys. Res., 98, 3093-3123 (1993).
51. Barnes, J. R., J.B. Pollack, R.M. Haberle, C.B. Leovy, R.W. Zurek, H. Lee, and J. Schaeffer, Mars atmospheric dynamics as simulated by the NASA Ames General Circulation Model. II - Transient baroclinic eddies, J. Geophys. Res., 98, 3125-3148 (1993).
52. Bougher, S.W., R.G. Roble, E.C. Ridley, and R.E. Dickinson, The Mars thermosphere. II - General circulation with coupled dynamics and composition, J. Geophys. Res., 95, 14811-14827 (1990).
53. Bougher, S.W., S. Engel, R.G. Roble, and B. Foster, Comparative terrestrial planet thermospheres. 2. Solar cycle variation of global structure and winds at Equinox, J. Geophys. Res., 95, 16591-16611 (1999).
54. Justus, C.G., D.L. Johnson, and B.F. James, A Revised Thermosphere for the Mars Global Reference Atmospheric Model (Mars-GRAM Version 3.4), NASA TM-108513, 1996.
55. Owen, T., K. Biemann, J.E. Biller, A.L. Lafleur, D.R. Rushneck, and D.W. Howarth, The composition of the atmosphere at the surface of Mars, J. Geophys. Res., 82, 4635-4639 (1977).
56. Levine, J.S., The Photochemistry of Atmospheres, Academic Press, New York (1985).
57. Smith, D.E., M.T. Zuber, S.C. Solomon, R.J. Phillips, J.W. Head, J.B. Garvin, W.B. Banerdt, D.O. Muhleman, G.H. Pettengill, G.A. Neumann, F.G. Lemoine, J.B. Abshire, O. Aharonson, D.C. Brown, S.A. Hauck, A.B. Ivanov, P.J. McGovern, H.J. Zwally, and T.C. Duxbury, The global topography of Mars and implication for surface evolution, Science, 284, 1495-1503 (1999).
58. Smith, D.E., and M.T. Zuber, The relationship between MOLA northern hemisphere topography and the 6.1-mbar atmospheric pressure surface of Mars, Geophys. Res. Lett., 25, 4397-4400 (1998).
59. Zuber, M.T., D.E. Smith, R.J. Phillips, S.C. Solomon, W.B. Banerdt, G.A. Neumann, and O. Aharonson, Shape of the northern hemisphere of Mars from the Mars Orbiter Laser Altimeter (MOLA), Geophys. Res. Lett., 25, 4393-4396 (1998).
60. Surkov, Yu.A., L.P. Moskalyova, O.S. Manvelian, A.T. Bazilyevsky, and V.P. Kharinkova, Geochemical interpretation of the results of measuring gamma-radiation of Mars, in Proceedings of 11th Lunar and Planetary Science Conference, pp. 669-676, Pergamon Press, New York (1980).
61. Surkov, Yu.A., V.L. Barsukov, L.P. Moskalyova, V.P. Kharinkova, and S.E. Zaitseva, Determination of the elemental composition of Martian rocks from Phobos 2, Nature, 341, 595-598 (1989).
62. Surkov, Yu.A., L.P. Moskalyova, M.Yu. Zolotov, V.P. Kharinkova, O.S. Manvelian, G.G. Smirnov, and A.V. Golovin, Phobos-2 data on Martian surface geochemistry, Geochem. Intern., 31, 50-58 (1994).
63. Toulmin, P., A.K. Baird, B.C. Clark, K. Keil, H.J. Rose, Jr., R.P. Christian, P.H. Evans, and W.C. Kelliher, Geochemical and mineralogical interpretation of the Viking inorganic chemical results, J. Geophys. Res., 84, 4625-4634 (1977).
64. Clark, B.C., A.K. Baird, R.J. Weldon, D.M. Tsusaki, L. Schnabel, and M.P. Candelaria, Chemical composition of Martian fines, J. Geophys. Res., 87, 10059-10067 (1982).
65. McSween, H. Y., Jr., S.L. Murchie, J.A. Crisp, N.T. Bridges, R.C. Anderson, J.F. Bell, III, D.T. Britt, J. Brckner, G. Dreibus, T. Economou, A. Ghosh, M.P. Golombek, J.P. Greenwood, J.R. Johnson, H.J. Moore, et al., Chemical, multispectral, and textural constraints on the composition and origin of rocks at the Mars Pathfinder landing site, J.Geophys.Res. 104, 8679-8716 (1999).
66. Bell, J.F. III, H.Y. McSween, Jr., J.A. Crisp,

R.V. Morris, S.L. Murchie, N.T. Bridges, J.R. Johnson, D.T. Britt, M.P. Golombek, H.J. Moore, A. Ghosh, J.L. Bishop, R.C. Anderson, J. Brckner, T. Economou, et al., Mineralogic and compositional properties of Martian soil and dust: results from Mars Pathfinder, J. Geophys. Res., 105, 1721-1756 (2000).

67. Grant, J.A., R. Arvidson, J.F. Bell, III, N.A. Cabrol, M.H. Carr, P. Christensen, L. Crumpler, D.J. Des Marais, B.L. Ehlmann, J. Farmer, M. Golombek, F.D. Grant, R. Greeley, K. Herkenhoff, R. Li, H.Y. McSween, D.W. Ming, J. Moersch, J.W. Rice, Jr., S. Ruff, L. Richter, S. Squyres, R. Sullivan, and C. Weitz, Surficial deposits at Gusev Crater along Spirit Rover traverses, Science, 305, 807-810 (2004).
68. Gellert, R., R. Rieder, R.C. Anderson, J. Brckner, B.C. Clark, G. Dreibus, T. Economou, G. Klingelhfer, G.W. Lugmair, D.W. Ming, S.W. Squyres, C. d'Uston, H. Wnke, A. Yen, and J. Zipfel, Chemistry of rocks and soils in Gusev Crater from the Alpha Particle X-ray Spectrometer, Science, 305, 829-832 (2004).
69. McSween, H.Y., R.E. Arvidson, J.F. Bell, III, D. Blaney, N.A. Cabrol, P.R. Christensen, B.C. Clark, J.A. Crisp, L.S. Crumpler, D.J. Des Marais, J.D. Farmer, R. Gellert, A. Ghosh, S. Gorevan, T. Graff, J. Grant, L.A. Haskin, K.E. Herkenhoff, J.R. Johnson, B.L. Jolliff, G. Klingelhoefer, A.T. Knudson, S. McLennan, K.A. Milam, J.E. Moersch, R.V. Morris, R. Rieder, S.W. Ruff, P.A. de Souza, Jr., S.W. Squyres, H. Wnke, A. Wang, M.B. Wyatt, A. Yen, and J. Zipfel, Basaltic rocks analyzed by the Spirit Rover in Gusev Crater, Science, 305, 842-845 (2004).
70. L.A. Soderblom, R.C. Anderson, R.E. Arvidson, J.F. Bell, III, N.A. Cabrol, W. Calvin, P.R. Christensen, B.C. Clark, T. Economou, B.L. Ehlmann, W.H. Farrand, D. Fike, R. Gellert, T.D. Glotch, M.P. Golombek, R. Greeley, J.P. Grotzinger, K.E. Herkenhoff, D.J. Jerolmack, J.R. Johnson, B. Jolliff, G. Klingelhfer, A.H. Knoll, Z.A. Learner, R. Li, M.C. Malin, S.M. McLennan, H.Y. McSween, D.W. Ming, R.V. Morris, J.W. Rice, Jr., L. Richter, R. Rieder, D. Rodionov, C. Schrder, F.P. Seelos, IV, J.M. Soderblom, S.W. Squyres, R. Sullivan, W.A. Watters, C.M. Weitz, M.B. Wyatt, A. Yen, and J. Zipfel, Soils of Eagle Crater and Meridiani Planum at the Opportunity Rover landing site, Science, 306, 1723-1726 (2004).
71. Rieder, R., R. Gellert, R.C. Anderson, J. Brckner, B.C. Clark, G. Dreibus, T. Economou, G. Klingelhfer, G.W. Lugmair, D.W. Ming, S.W. Squyres, C. d'Uston, H. Wnke, A. Yen, and J. Zipfel, Chemistry of rocks and soils at Meridiani Planum from the Alpha Particle X-ray Spectrometer, Science, 306, 1746-1749 (2004).
72. Brckner, J., G. Dreibus, G.W. Lugmair, R. Rieder, H. Wnke, and T. Economou, Chemical composition of the Martian surface as derived from Pathfinder, Viking, and Martian Meteorite data, in Proceedings of 30th Lunar and Planetary Science Conference, pp. 1250 (abstract), Houston TX (1999).
73. Tanaka, K.L., and D.H. Scott, Geologic Map of the Polar Regions of Mars (scale 1:15000000), USGS Misc. Inv. Series Map I-1802-C (1987).
74. Kahn, R., Some observational constraints on the global-scale wind system on Mars, J. Geophys. Res., 88, 10189-10209 (1983).
75. Christensen, P.R., and R.W. Zurek, Martian north polar hazes and surface ice: results from the Viking survey/completion mission, J. Geophys. Res., 89, 4587-4596 (1984).
76. Thomas, P.C., J. Veverka, and R. Campos-Marquetti, Frost streaks in the south polar cap of Mars, J. Geophys. Res., 84, 4621-4633 (1979).
77. James, P.B., K.M. Malolepszy, and L.J. Martin, Interannual variability of Mars' south polar cap, Icarus. 71, 298-305 (1987).
78. Wilson, J. W., F.F. Badavi, F.A. Cucinotta, J.L. Shinn, G.D. Badhwar, R. Silberberg, C.H. Tsao, L.W. Townsend, and R.K. Tripathi, HZETRN: Description of a Free-Space Ion and Nucleon Transport and Shielding Computer Program, NASA TP-3495 (1995).
79. De Angelis, G., F.F. Badavi, J.M. Clem, S.R. Blattnig, M.S. Clowdsley, J.E. Nealy, R.K.

Tripathi, and J.W. Wilson, A time-dependent model for the lunar radiation environment, Paper SAE-2005-01-2831, pp. 1-11, Society for Automotive Engineering (SAE) (2005).
80. J.M. Clem, G. De Angelis, P. Goldhagen, and J.W. Wilson, Preliminary validation of computational procedures for a new Atmospheric Ionizing Radiation (AIR) model, Adv. Space Res., 32(1), 27-33 (2003).
81. Saganti, P.K., F.A. Cucinotta, J.W. Wilson, L.C. Simonsen, and C.J. Zeitlin, Radiation climate map for analyzing risks to astronauts on the Mars surface from galactic cosmic rays, Space Scie. Rev., 110, 143-156 (2004).